Nuclear Instruments and Methods in Physics Research A 823 (2016) 98–106

Contents lists available at ScienceDirect

Nuclear Instruments and Methods in Physics Research A

journal homepage: www.elsevier.com/locate/nima

Study of accuracy in the position determination with SALSA, a γ-scanning system for the characterization of segmented HPGe detectors

A. Hernandez-Prieto [a,*], B. Quintana [a], S. Martìn [a], C. Domingo-Pardo [b]

[a] Laboratorio de Radiaciones Ionizantes, Departamento de Física Fundamental, Universidad de Salamanca, C \Espejo s/n, Salamanca, Spain
[b] Instituto de Física Corpuscular, C \Catedrático José Beltrán, 2, Paterna, Spain

ARTICLE INFO

Article history:
Received 19 December 2014
Received in revised form
21 February 2016
Accepted 31 March 2016
Available online 6 April 2016

Keywords:
γ-Camera
Virtual collimation
SAlamanca Lyso-based Scanning Array (SALSA)
Segmented HPGe detectors

ABSTRACT

Accurate characterization of the electric response of segmented high-purity germanium (HPGe) detectors as a function of the interaction position is one of the current goals of the Nuclear Physics community seeking to perform γ-ray tracking or even imaging with these detectors. For this purpose, scanning devices must be developed to achieve the signal-position association with the highest precision. With a view to studying the accuracy achieved with SALSA, the SAlamanca Lyso-based Scanning Array, here we report a detailed study on the uncertainty sources and their effect in the position determination inside the HPGe detector to be scanned. The optimization performed on the design of SALSA, aimed at minimizing the effect of the uncertainty sources, afforded an intrinsic uncertainty of ~2 mm for large coaxial detectors and ~1 mm for planar ones.

1. Introduction

The new γ-ray position sensitive HPGe detectors are essential tools to perform γ spectroscopy at the new Radioactive-Ion Beam (RIB) facilities. The main improvement in these devices is achieved by the high segmentation of their electrical contacts, which are responsible for collecting the charge carriers released in each photon interaction. Some relevant examples of these detectors can be found in international collaborations such as AGATA [1] or GRETA [2]. High-contact segmentation enables the interaction points of a γ ray inside the HPGe crystal to be determined, thereby providing the data needed to reconstruct the γ-ray track. However, as an intermediate step, it is necessary to characterize the electrical response of the HPGe crystal with respect to the position of the interaction point. At the same time, in order to explore in depth the capabilities of segmented HPGe detector, maximum precision in its characterization must be achieved. SALSA, which is the acronym of the SAlamanca Lyso-based Scanning Array, was designed specifically to reduce the sources of uncertainty involved in the position determination inside the HPGe crystal. This determination is based on virtual collimation [3], where two collinear 511-keV photons emitted in the annihilation of a positron are used. This method also needs a Pulse Shape Analysis Comparison (PSAC) algorithm [4] to achieve the three-dimensional (3D) position determination in the HPGe detector to be scanned. Previous characterization devices based in the same principles as SALSA have been developed and tested [5,6].

The optimized design of SALSA, aimed at improving the final accuracy, consists of a high-spatial-resolution γ camera with large field of view and a point-like ^{22}Na source, both mounted on a high-precision mechanical structure which allows to make 90° rotations of the whole ^{22}Na source and γ camera around the HPGe detector to scan and also to adjust the distance between ^{22}Na source and detector in order to reduce the influence of the uncertainty sources in the calculation of position.

Here, we analyse the design of the scanning system in detail, together with its sources of uncertainty and how these determine the total uncertainty of the final position in the HPGe crystal. The effect of distance between detectors and ^{22}Na source is evaluated through the uncertainty values obtained for different detectors: an AGATA-type highly segmented coaxial HPGe detector and a segmented planar prototype designed for the DESPEC experiment [7]. First, however, in Section 2 we shall describe SALSA, introducing its components. In Section 3, the algorithm utilized to calculate the interaction position inside the HPGe detector as a function of known parameters is discussed. In Section 4 the global system of reference in SALSA is defined and all the elements placed on it.

* Corresponding author.
E-mail address: alvaro.prieto@usal.es (A. Hernandez-Prieto).

http://dx.doi.org/10.1016/j.nima.2016.03.103
0168-9002/

In Sections 5 and 6 the uncertainties inherent to both, ^{22}Na source and γ camera are evaluated. In Section 7, the total uncertainty provided by SALSA in position determination is calculated for the cases of interest. In Section 8, an experimental validation of position determination and its corresponding uncertainty evaluation is performed with a conventional HPGe detector. Finally, in Section 9, we offer some conclusions.

2. The SALSA setup

As mentioned above, the main elements of SALSA are a high-spatial-resolution γ camera, a point-like ^{22}Na source and the mechanical platform supporting these two elements together with the detector to be scanned. All these elements, together with the associated electronics, aim to obtain the HPGe electric signals, each one associated to an interaction point within the HPGe crystal. Therefore, the main challenge of SALSA is to determine the real interaction points with minimum uncertainty. The radioactive source used generates two 511 keV γ rays coming from the annihilation of the β^+ emitted in the disintegration of the ^{22}Na with a nearby electron. The source is provided by Eckert and Ziegler Company [8] and it consists of a ^{22}Na (0.125-mm-radius spherical active volume) with a nominal activity of 1 MBq, encapsulated in a 25.4-mm-diameter disk made with carbon epoxy fibre. Its small active volume and the encapsulation are suitable for achieving maximum accuracy in the initial positioning of the γ rays generated in the source.The γ camera is placed in front of the ^{22}Na source to measure one of the 511 keV γ rays generated in each e^-e^+ annihilation. It consists of four high-spatial-resolution detectors coupled optically, each one made up by a continuous lutetium yttrium oxyorthosilicate (LYSO) scintillating crystal [9], $52\times52\times5$ mm^3 size. The readout of each crystal is performed by a pixelated position-sensitive photomultiplier tube (PSPMT) from Hamamatsu, model H10966A-100. The junction of the four crystals provides a large field of view (104×104 mm^2) suitable for scanning, in just one shot, large-sized HPGe detectors with no detriment to accuracy. Their role is to provide the interaction point of the 511 keV γ ray in the γ camera detected in coincidence with the other 511 keV γ ray interacting in the HPGe crystal. This point in the γ camera is referred to as (X_L, Y_L, Z_L). Subsequently, the direction of the γ ray detected is determined using this point and the generation point of the two γ rays in the ^{22}Na source. The latter is referred to as (X_S, Y_S, Z_S) and is generally located inside the ^{22}Na source, as demonstrated below. Both points correspond to the same reference system, which is placed in the centre of the detector to be scanned.

Assuming that the β^+ particle annihilates at rest, the incident direction of the γ ray interacting in the HPGe crystal can be obtained from the direction of the γ ray detected in the γ camera. The non-collinearity of the two photons resulting from the e^+e^- annihilation has been studied by several authors [10,11]. The dimensions of SALSA, given below, and the high energy resolution of HPGe detectors allow us to disregard its effect. Therefore, the direction of the γ ray interacting in the HPGe crystal will be given by the straight line defined by the two cited points, which are shown in Fig. 1, satisfying the following well-known equation:

$$\frac{X - X_S}{X_L - X_S} = \frac{Y - Y_S}{Y_L - Y_S} = \frac{Z - Z_S}{Z_L - Z_S}. \quad (1)$$

The structure that attaches ^{22}Na source and γ camera, linking one to the other in the same branch and allowing them to be placed in a common reference system, is the SALSA mechanical structure. Fig. 2 shows the complete SALSA setup when scanning a BEGe detector.

This structure enables us to scan a HPGe crystal from two different positions, called S_1 and S_2. These two positions are needed to obtain a single point of interaction in the HPGe crystal and not just one direction. Fig. 1 graphically shows the two scanning positions of SALSA. All the elements employed in the SALSA support platform were made at high-precision machining workshops. The γ camera housing and the ^{22}Na source support structure are machined with 0.2 mm and 0.1 mm precision, respectively. The structure to locate the linear and circular motion circuit and the HPGe detector was from Hepcomotion ® [12]. For this structure, MCS ® aluminium profiles with 0.1 mm precision cuts were employed. In order to construct a motion circuit, the PRT^2 technology also from Hepcomotion ® was used. It allows the ^{22}Na source and γ camera set to be moved around the HPGe detector with high accuracy from the so-called S_1 scan stage to the 90° rotated S_2 one.

Fig. 3 shows the layout of both the linear and circular motion circuits. The mechanical structure enables the distance both between ^{22}Na source and γ camera and between ^{22}Na source and HPGe detector to be adjusted. ^{22}Na source and γ camera are placed on two carriages that can move linearly with respect to each other on the same branch. Once distances are adjusted, the carriages are blocked and the set can rotate $(90 \pm 0.03)^\circ$ in order to change the scanner position from S_1 to S_2. In SALSA, ^{22}Na source and γ camera have their own relative reference system. The one corresponding to the ^{22}Na source is defined at the geometrical centre of its active volume and a position located on it is denoted as (X''_S, Y''_S, Z''_S). The one corresponding to the γ camera is defined at the geometrical centre of its detection plane and a point located on it is denoted as

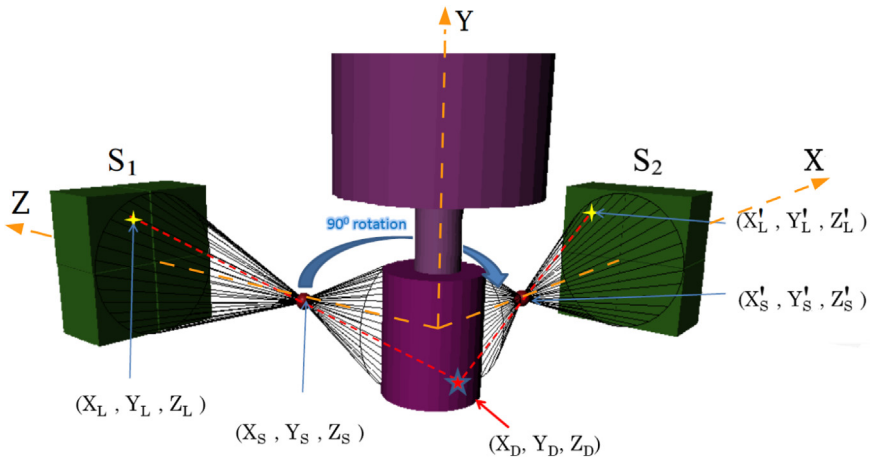

Fig. 1. Schematic for SALSA. The HPGe detector to scan is depicted in purple, whereas the γ camera is in green. The point-like ^{22}Na source is drawn red and the γ cones generated are in black. (For interpretation of the references to colour in this figure caption, the reader is referred to the web version of this paper.)

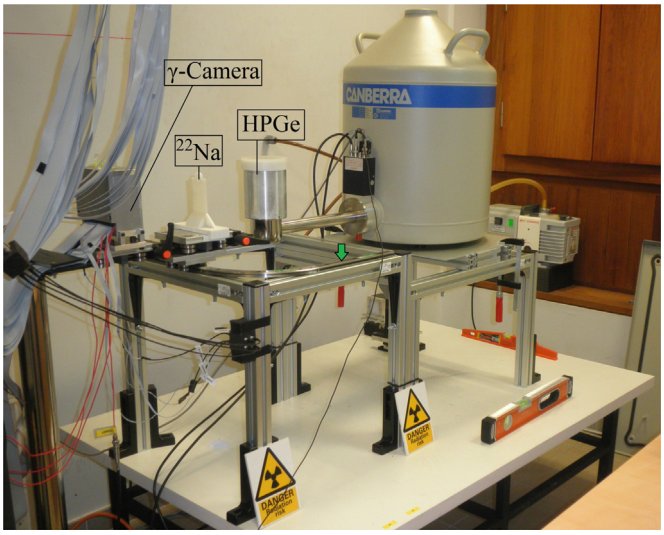

Fig. 2. Picture of SALSA with a BEGe detector placed to be scanned. The γ-camera and ^{22}Na source are set in the scan position S_1. The second scan stage S_2 is indicated by a green arrow. The rest of the elements of SALSA are also pointed in the picture. (For interpretation of the references to colour in this figure caption, the reader is referred to the web version of this paper.)

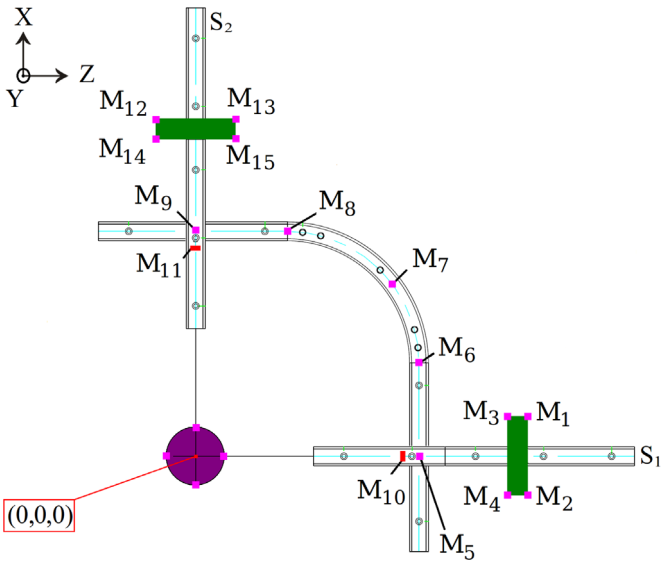

Fig. 3. Schematics of the SALSA mechanics. All vertical marks obtained are indicated for both S_1 and S_2 positions. In green the γ camera is represented while the red colour indicates the ^{22}Na source support. The scanned detector is also placed in the schema. (For interpretation of the references to colour in this figure caption, the reader is referred to the web version of this paper.)

(X_L'', Y_L'', Z_L'').

However, the positions of interest in these two elements must be referred to the global SALSA reference system. This is achieved by a translation, and hence it is necessary to determine the mechanical positions of ^{22}Na source and γ camera in the mechanical structure with respect to the global system of reference. At the same time, uncertainties in the positioning of the two elements must be evaluated. These uncertainties correspond both to the mechanical accuracy and to the method employed to measure the absolute positions of the different elements of the mechanics. For the Y coordinate, a set of measurements of the vertical mark of each SALSA component was done using a Leica Total Station TPS$_1$200, which has a precision of 0.7 mm/km. Since the measurements were taken by looking at a 0.25 mm calibrated rule, this is assumed to be the accuracy of these measurements. The

Table 1
Measured vertical dimension mark in different points in SALSA.

Position	Vertical mark (mm)	Mean value (mm)
M_5	395.90 ± 0.25	$M_{MEC} = 395.80 \pm 0.25$
M_6	395.80 ± 0.25	
M_7	395.80 ± 0.25	
M_8	395.80 ± 0.25	
M_9	395.70 ± 0.25	
M_1	175.80 ± 0.25	$M_H = 175.85 \pm 0.25$
M_2	175.90 ± 0.25	
M_3	175.80 ± 0.25	
M_4	175.90 ± 0.25	
M_{10}	238.30 ± 0.25	$M_S = 238.30 \pm 0.25$
M_{11}	238.30 ± 0.25	$M_S' = 238.30 \pm 0.25$
M_{12}	176.00 ± 0.25	$M_H' = 175.95 \pm 0.25$
M_{13}	175.90 ± 0.25	
M_{14}	176.00 ± 0.25	
M_{15}	175.90 ± 0.25	

different measurements made are shown in Fig. 3 and their results listed in Table 1. With M_1 up to M_4 we refer to the measurements taken on the top of the γ camera housing in S_1. The measurements taken on several points of the motion circuit go from M_5 to M_9. With M_{10} and M_{11}, we refer to the measurements taken on the ^{22}Na source support in S_1 and S_2. Finally, M_{12}, M_{13}, M_{14} and M_{15} correspond to the four vertical marks located on the top of the γ camera housing when placed in S_2. For every set of measurements the mean value is calculated, being its uncertainty driven by systematic uncertainty introduced by the inaccuracy in the vertical mark measurements. This data is used in Section 4, where the translation from the different coordinate systems to the global one is determined.

3. Principles of the position determination in SALSA

The first step in the position determination is to calculate the incident directions of the γ rays in the HPGe crystal, using Eq. (1) together with the interaction position in the γ camera (X_L, Y_L, Z_L) and the annihilation point in the ^{22}Na source (X_S, Y_S, Z_S). This is performed first in the so-called S_1 configuration, which provides a set of γ-ray tracks, each with a certain associated electrical response in the HPGe crystal. Then, the ^{22}Na source plus γ camera system is rotated 90° around the HPGe detector axis to the so-called S_2 configuration, where another set of γ-ray tracks is obtained, together with their associated electrical responses in the HPGe crystal. In S_2, the γ-ray interaction position into the γ camera is denoted as (X_L', Y_L', Z_L'), while the position of the generation point of the two γ rays is referred to as (X_S', Y_S', Z_S'), as seen in Fig. 1. Consequently, the direction of the γ-path in S_2 will be defined by a straight line equation given by Eq. (1) but replacing the points corresponding to S_1 by their equivalent ones in S_2. The electrical response associated to each track correspond to an unknown interaction point in the HPGe placed on the track. In order to obtain this interaction point accurately, two tracks, one in each configuration, that enclose the same interaction point in the HPGe detector must be found by using all the data from S_1 and S_2. To decide that two tracks correspond to the same interaction point, it is necessary to compare the two electrical responses associated to each track statistically. The design of the HPGe segmented detectors ensures that every position in the crystal will give a unique

electrical response by looking not only at the segment where the gamma has interacted, but also at the surrounding ones. The induced signals in the neighbouring segments allow us to distinguish where the γ ray has interacted within the segment [1]. The statistical comparison is achieved by the PSAC algorithm developed in our laboratory which uses a Wilcoxon signed-rank test [13]. Once checked, the crossing point of the two tracks in S_1 and S_2 corresponding to the same interaction point in the HPGe crystal, which is referred to as (X_D, Y_D, Z_D), is obtained from the following two equations:

$$\frac{(X_D - X_S)}{(X_L - X_S)}(Z_L - Z_S) + Z_S = \frac{(X_D - X'_S)}{(X'_L - X'_S)}(Z'_L - Z'_S) + Z'_S \tag{2}$$

$$\frac{(Z_D - Z_S)}{(Z_L - Z_S)}\left(Y_L - Y_S\right) + Y_S = \frac{(Z_D - Z'_S)}{(Z'_L - Z'_S)}\left(Y'_L - Y'_S\right) + Y'_S. \tag{3}$$

Solving this set of equations, the crossing point is obtained as:

$$X_D = \frac{\frac{X_S(Z_L - Z_S)}{X_L - X_S} - Z_S + Z'_S - \frac{X'_S(Z'_L - Z'_S)}{X'_L - X'_S}}{\frac{(Z_L - Z_S)}{X_L - X_S} - \frac{(Z'_L - Z'_S)}{X'_L - X'_S}} \tag{4}$$

$$Z_D = \frac{(X_D - X_S)}{(X_L - X_S)}(Z_L - Z_S) + Z_S \tag{5}$$

$$Y_D = \begin{cases} \dfrac{(Z_D - Z_S)}{(Z_L - Z_S)}(Y_L - Y_S) + Y_S \quad (Line1) \\ \dfrac{(Z_D - Z'_S)}{(Z'_L - Z'_S)}(Y'_L - Y'_S) + Y'_S \quad (Line2) \end{cases}. \tag{6}$$

From Eqs. (4) and (5), X_D and Z_D are calculated. Eq. (6) constitutes the geometrical condition to determine the paths from S_1 and S_2 which correspond to the same interaction point inside the HPGe crystal (X_D, Y_D, Z_D). Additionally, a further check is made to this solution: the point must be located in the HPGe crystal.

Regarding the uncertainty associated with the position determination of the interaction point in the HPGe crystal, it is assumed that a negligible uncertainty is introduced by the PSAC algorithm as shown in Section 8. Consequently, the uncertainty in the determination of this point will mainly come from the data needed to calculate the two crossing tracks: the position of the interaction point in the γ camera and the position of the annihilation point within the ^{22}Na source, both in S_1 and S_2.

4. Determination of the coordinates in the SALSA global reference system

To solve Eqs. (4)–(6), the points corresponding to the interaction point in the γ camera (X_L, Y_L, Z_L) in S_1 and (X'_L, Y'_L, Z'_L) in S_2, and to the ^{22}Na source emission point, (X_S, Y_S, Z_S) in S_1 and (X'_S, Y'_S, Z'_S) in S_2, must be calculated. The calculation involves the translation of these points initially obtained in the reference systems of the γ camera and the ^{22}Na source to a common one. The global reference system chosen for SALSA has its origin in the centre of the HPGe crystal and defined by the SALSA mechanical structure (see Fig. 1). The reference system of the ^{22}Na source has its origin at the geometrical centre of its active volume, which corresponds to (X_{SO}, Y_{SO}, Z_{SO}) in the global reference system. Likewise, the reference system of the γ camera is defined at the geometrical centre of its detection plane and is referred to as (X_{CO}, Y_{CO}, Z_{CO}) in the global reference system. The translation requires the translation vectors from the individual reference systems to the global one to be known, but this simply involves calculating the coordinates of the origin of each local reference system in the global one.

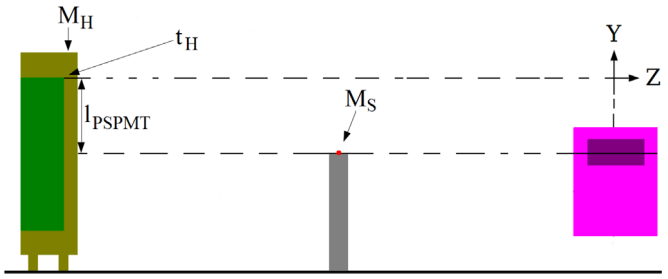

Fig. 4. Lateral view of SALSA mechanics. From left to right, the γ camera, the ^{22}Na source and the HPGe crystal. For the γ camera, the brown colour indicates the housing and the green one the γ camera itself. The red colour is used for the ^{22}Na source and grey one for its support. (For interpretation of the references to colour in this figure caption, the reader is referred to the web version of this paper.)

Starting with the Y coordinate, a set of measurements was performed with the total station described in Section 2. Since the level measurements are relative to external components, some calculations must be made in order to evaluate the Y coordinate of both the centre of the γ camera and the ^{22}Na source. In Fig. 4, the position of the marks on the γ camera and ^{22}Na source are indicated. For the γ camera, the magnitudes that link the marks with its centre are also shown.

As can be seen in Fig. 4, the Y coordinate regarding of the centre of the γ camera (Y_{CO}) can be obtained as follows:

$$Y_{CO} = M_H + t_H + l_{PSPMT} \tag{7}$$

where M_H is the averaged value of the vertical mark given in Table 1 for the γ-camera housing, t_H is the thickness of the housing, its value being (10.0 ± 0.2) mm, and l_{PSPMT} is the semi-length of the γ camera determined by the PSPMT size, its value being (52.00 ± 0.15) mm. Consequently, the position of the centre in the γ camera referred to the SALSA system of reference becomes $Y_{CO} = (237.85 \pm 0.35)$ mm for S_1 and $Y'_{CO} = (237.95 \pm 0.35)$ mm for S_2. The total uncertainties of these values $(\sigma_{Y_{CO}})$ were evaluated by propagating all the components involved in Eq. (7). Regarding the ^{22}Na source, the position of its active volume centre is matched to the top of the support structure by construction. Therefore, no further calculation is needed to obtain the Y coordinate of the centre of the source, although this is necessary in the case of its uncertainty. This uncertainty is affected by two factors. The first one is the machining of the support structure, which is made with a precision of ±0.1 mm. The second one is the vertical dimension mark measurement M_S for S_1 and M'_S for S_2, whose values are shown in Table 1. Therefore, the Y coordinate of the centre of the ^{22}Na source is $Y_{SO} = (238.30 \pm 0.27)$ mm for S_1 and $Y'_{SO} = Y_{SO}$ for S_2, whose uncertainties are calculated by propagating the two contributions. When the deviation, δ, between the centre of the ^{22}Na source and the position of the centre in the γ camera is calculated for S_1 and S_2, it is seen that both values do not differ statistically. Therefore, taking into account that $Y_{SO} = Y'_{SO}$, ^{22}Na source and γ camera rotates in the XZ plane of the global reference system. This fact avoids further corrections in the position calculation. Regarding the X coordinate, in the S_1 scanning position the uncertainty is purely mechanical, because no level measurements are needed to establish their values with respect to the global reference system. Fig. 5 shows a frontal view of the γ camera and ^{22}Na source system. The high-precision machining allows the absence of systematic deviation to be assumed. Therefore, according to Fig. 5, $X_{CO} = X_{SO} = 0$.

For the X coordinate, there are three sources of uncertainty in the determination of the γ camera centre: The first one corresponds to the uncertainty in the positioning of the housing of the γ

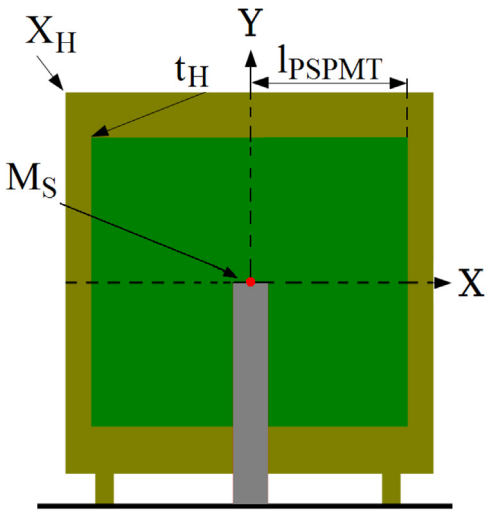

Fig. 5. Frontal view of the layout of SALSA mechanics. The brown colour indicates the housing and the green one the γ camera itself, while the red colour is used for the ^{22}Na source and the grey one for its support. (For interpretation of the references to colour in this figure caption, the reader is referred to the web version of this paper.)

camera in the mechanics. Owing to the high-precision machining, this value is ±0.2 mm. The second one comes from the positioning of the four LYSO detectors inside the housing, which is also ±0.2 mm. The last one is the semi-length of the PSPMT, with an uncertainty of ±0.15 mm given by the manufacturer. By propagation, the uncertainty value for X_{CO} is ±0.32 mm. Therefore, the coordinate of the centre of the γ camera in the global system of reference becomes $X_{CO} = (0.00 \pm 0.32)$ mm.

Regarding the ^{22}Na source, the uncertainty in the X coordinate of its centre comes, on the one hand, from the uncertainty of the machining of the support structure, which is ±0.1 mm, and, on the other hand, from the uncertainty to position the support structure in the high-precision mechanics, which is ±0.2 mm. As a consequence of the uncertainty propagation, the X coordinate of the geometrical centre of the source in the SALSA system is $X_{SO} = (0.00 \pm 0.22)$ mm.

In the scanning position S_2, the rigid bar where ^{22}Na source and γ camera are placed becomes X-axis. Therefore, X becomes Z in the frontal view of Fig. 5. Consequently, $Z'_{CO}=X_{CO}$ and $Z'_{SO}=X_{SO}$ as γ camera and ^{22}Na source are tightly attached to the rigid bar.

Regarding the third component of γ camera and ^{22}Na source centres, Z in S_1 and X in S_2, $X'_{CO} = Z_{CO}$ and $X'_{SO} = Z_{SO}$ because, as said above, both elements are attached to the rigid scanning branch. However, to obtain the precise value of these coordinates it is necessary to take into account that distances between HPGe detector and the elements of the branch are adjusted depending on the size of the detector to be scanned. The distances taken into account in the calculation of Z_{SO} (X'_{SO}) and Z_{CO} (X'_{CO}) are shown in Fig. 6. There are two: the distance d along Z in S_1 (X in S_2) between the centre of the ^{22}Na source and the centre of our global system

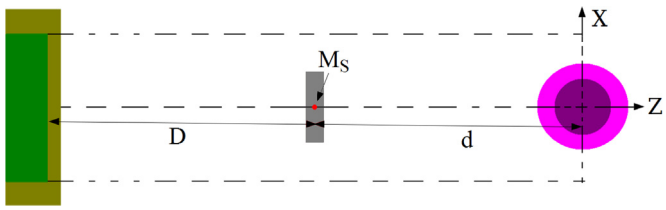

Fig. 6. Up view of the layout of SALSA mechanics. The colours to represent the different elements are the same as presented in previous figures. (For interpretation of the references to colour in this figure caption, the reader is referred to the web version of this paper.)

of reference and the distance D along Z in S_1 (X in S_2) between the centre of the ^{22}Na source and the external surface of the γ camera. Therefore, $Z_{SO}=d$ and $Z_{CO} = d + D + w$, where w is the distance along Z between the external window surface and the geometrical centre of the γ camera. D and d are selected according to the size of the HPGe detector, as mentioned above.

An example is studied in order to show the values, together with their uncertainties, obtained in some relevant cases. One might be the characterization, already performed, of a BEGe detector. In the configuration shown in Fig. 6, a calibrated ruler with 0.5 mm precision was used to determine D and d values. The results are $d = (188.5 \pm 0.5)$ mm and $D = (188.5 \pm 0.5)$ mm. The quoted uncertainties are obtained by propagating the accuracy of the ruler (±0.5 mm) and the uncertainties both in the machining of the support structure (±0.1 mm) for the ^{22}Na source and in the machining of the housing (±0.2 mm) for the γ camera. Finally, $Z_{SO} = (188.5 \pm 0.5)$ mm and $Z_{CO} = (379.5 \pm 0.7)$ mm, the same values being, respectively, for X'_{SO} and X'_{CO} in S_2.

Now, all the elements of SALSA are referred to a common system of reference and, therefore, any point within these elements can be referred to the global reference system. As a previous step, the points of interest in ^{22}Na source and γ camera reference system need to be known. This task is explained in the two following sections, also evaluating the intrinsic uncertainty associated with each point.

5. The β^+ annihilation position and its uncertainty

The annihilation position (X_S, Y_S, Z_S) is needed to solve Eqs. (4)–(6) and, consequently, to obtain the interaction point (X_D, Y_D, Z_D) in the scanned detector. The specific objectives of this section are to reach the best estimation of the annihilation point coordinates for all the γ rays emitted by the source and to estimate the associated uncertainty.

As stated above, the two γ rays from the ^{22}Na source come from the annihilation of the emitted positron with one surrounding electron. However, prior to this, the positron travels a certain distance through the material. Therefore, the two γ-rays generation point is located at the positron track's end-point. The uncertainty in the determination of its coordinates becomes a degradation factor in the scanning system because these coordinates cannot be known [3]. A Monte Carlo (MC) simulation was performed in order to obtain the spatial distribution of the annihilation points, in which the relevant characteristics of the source were implemented. The statistical distribution corresponding to each coordinate enables us to determine the mean point and the uncertainty of each annihilation coordinate.

The MC simulation was performed using the Geant4 toolkit [14,15]. Its goal is to evaluate the length that the positron coming from the ^{22}Na decay travels through the source material until it annihilates with one surrounding electron to generate the two collinear γ rays.

A sphere with 0.25 mm diameter of ^{22}Na, as described in Section 2, with all the processes and decay probabilities inherent to this radionuclide was implemented in the MC code. The annihilation position was recorded event by event, which enables us to know its coordinates (X''_S, Y''_S, Z''_S) for each β^+ in the reference system of the ^{22}Na source, obtaining the projection on the XY plane shown in Fig. 7. When representing the probability distribution corresponding to X''_S coordinate (see Fig. 8) a profile centred at zero was obtained. The same ones were obtained for Y''_S and Z''_S, as expected according to the symmetry of the ^{22}Na source.

In order to calculate the standard deviation of X''_S, Y''_S and Z''_S distributions, a numerical calculation was performed by using Mathematica [16]. With this tool, an interpolation was made using

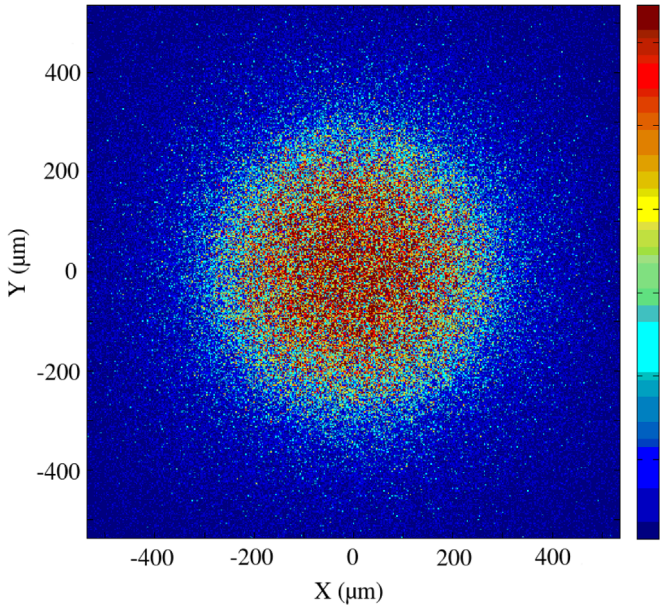

Fig. 7. 2D projection of annihilation position inside the ^{22}Na source.

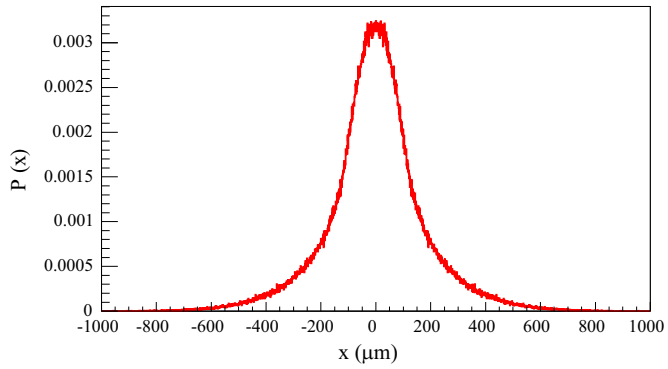

Fig. 8. Histogram of the probability distribution for X_S^s. The same one is obtained for Y_S'' and Z_S'' coordinates.

the statistical distribution data to obtain a functional expression of the probability density, $P(x)$, which allowed us to calculate the mean value of x numerically by the well-known integral definition:

$$\bar{x} = \int_0^\infty xP(x)\,dx. \tag{8}$$

Its standard deviation was also calculated numerically by using its definition in the descriptive statistics, which has the following formula:

$$\sigma^2 = \int_0^\infty (x-\bar{x})^2 P(x)\,dx. \tag{9}$$

The results obtained for the probability distributions associated with the coordinates (X_S'', Y_S'', Z_S'') of the annihilation point are listed in Table 2, where the mean is given in the first column, the standard deviation σ in the second one and the percentage area enclosed in the interval $\bar{x} \pm \sigma$ in the third one.

Table 2
Mean ($\bar{x}$) and standard deviation (σ) values obtained for the coordinates of annihilation point X_S'', Y_S'' and Z_S''. A (%) is the relative area comprised in the interval $\bar{x} \pm \sigma$.

Coordinate	$\bar{x}$ (mm)	σ (mm)	A (%)
X_S''	0.00	0.19	78.2
Y_S''	0.00	0.19	77.6
Z_S''	0.00	0.19	78.1

As observed in Table 2, the best estimation for the annihilation position (X_S'', Y_S'', Z_S'') is the geometrical centre of the ^{22}Na source. Therefore, we took $\sigma_{X_S''} = \sigma_{Y_S''} = \sigma_{Z_S''} = \pm 0.19$ mm as uncertainty in the coordinates (X_S'', Y_S'', Z_S'').

Given the non-Gaussian condition of the distribution, the coverage area is 78%. In order to make the result of the uncertainty compatible with the rest of the work presented here, a coverage factor, $k=1.36$, is needed to be introduced on the basis of the desired level of confidence of 68%. This coverage factor will allow us to redefine the uncertainty in each coordinate as $err(\xi_i) = 0.14$ mm, where ξ_i represents each X, Y and Z coordinates. Thus, the annihilation point or γ-ray emission point taken in the calculation of the γ-ray track is $X_S'' = Y_S'' = Z_S'' = (0.00 \pm 0.14)$ mm.

6. The γ-camera interaction points and their uncertainty

An interaction point in the γ camera measured during the scanning process, (X_L'', Y_L'', Z_L''), is given by the image reconstruction algorithm specifically developed for our γ camera, whose results are shown in a previous work [17]. Actually, the algorithm only determines the components of the plane of the γ camera that faces the ^{22}Na source, which are X_L'' and Y_L'' in S_1 and Z_L'' and Y_L'' in S_2, together with their corresponding uncertainties. Although the uncertainty values are estimated event by event, a value of 0.4 mm is taken in this work for estimation purposes. This value was obtained in the work mentioned above. Regarding the third component Z_L'' (X_L'' in S_2), no information was obtained from the analysis of the signal measured in the γ camera owing to the reduced thickness of the LYSO crystal. Therefore, a MC simulation was performed with Geant4 to obtain an estimation of the value of this coordinate, together with its uncertainty.

The absorption probability for 511 keV γ rays for the third coordinate versus the Z coordinate of the interaction position point in the γ camera is shown in Fig. 9. The probability shape is a consequence of the fact that the linear attenuation factor in the LYSO material is 0.87 cm^{-1} at 511 keV, which corresponds to a mean free path of 1.15 cm for γ rays at this energy. Accordingly, what is shown in Fig. 9 is a truncated exponential distribution. For this type of distributions the functional expression of the probability density, $P(x)$, has been studied in depth in [18,19]. Using it in Eqs. (8) and (9), the mean value for the distribution is $Z_L'' = (2.31 \pm 1.43)$ mm. This value will be applied to evaluate the total uncertainty in the position determination inside the HPGe crystal. Therefore, the interaction position in S_1 of a particular γ ray in the γ camera plane can be defined as

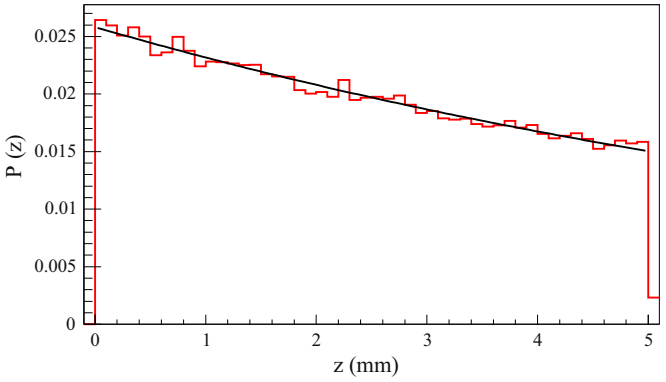

Fig. 9. Histogram of the probability distribution of the absorption position for γ rays along the perpendicular axis in LYSO crystal. In black the exponential fit.

$(X_L'' \pm \sigma_{X_L}'', Y_L'' \pm \sigma_{Y_L}'', Z_L'' \pm \sigma_{Z_L}'')$, being $\sigma_{X_L}'' = \sigma_{Y_L}'' \sim \pm 0.4$ mm and $\sigma_{Z_L}'' = \pm 1.43$ mm in the reference coordinate system centred in the γ camera. The same situation will be seen in S_2, but in that case $\sigma_{Z_L}'' = \sigma_{Y_L}'' \sim \pm 0.4$ mm and $\sigma_{X_L}'' = \pm 1.43$ mm.

7. Total uncertainty in SALSA

Once the points needed in the calculation of Eqs. (4)–(6) have been determined in the previous sections and their uncertainties calculated taking into account all the sources of uncertainty, an estimation of the uncertainties corresponding to (X_D, Y_D, Z_D) can be made. From Eqs. (4)–(6), the uncertainty at a certain point (X_D, Y_D, Z_D) can be evaluated by doing uncertainty propagation. This uncertainty is affected by the β^+ annihilation position in the ^{22}Na source seen in Section 5, the spatial resolution in the γ camera given in Section 6, and also by the contribution generated by the translation required to transform the reference systems for both elements into the common reference system defined by the SALSA mechanics in Section 4. Accordingly, the calculation of the total uncertainty in X_D, Z_D and Y_D can now be done taking into account the uncertainties of all the variables. Regarding the Y coordinate, the total uncertainty of Y_L (Y coordinate of interaction in the γ-camera plane), becomes $\sigma_{Y_L} = \pm 0.53$ mm after propagation in the translation formula. The total uncertainty of Y_S (Y coordinate of the ^{22}Na source annihilation point) is $\sigma_{Y_S} = \pm 0.30$ mm.

For the X (Z in S_2) coordinate, the total uncertainty of X_L in S_1 (Z_L in S_2) can be expressed as a propagation of the uncertainty in the position of the centre of the γ camera and its image resolution in this coordinate. Therefore, $\sigma_{X_L} = \pm 0.51$ mm. For X_S in S_1 (Z_S in S_2), the uncertainty value σ_{X_S} (σ_{Z_S} in S_2) becomes $\sigma_{X_S} = \pm 0.26$ mm.

With respect to Z coordinate (X in S_2) the coordinate Z_L in S_1 (X_L in S_2) of the interaction point has an uncertainty σ_{Z_L} (σ_{X_L}) of 1.61 mm, obtained after propagating the uncertainty in the position of the centre of the γ camera (Z_{CO}) and Z_L'' uncertainties. The Z_S in S_1 (X_S in S_2) uncertainty of the 511 keV γ emission point is σ_{Z_S} (σ_{X_S} in S_2) equal to ± 0.52 mm, obtained when considering the uncertainty in the position range and in the positioning of the ^{22}Na source.

Once the uncertainties for all the parameters involved in calculation of the interaction position inside the HPGe crystal had been obtained explicitly in the SALSA reference system, the last step was to perform uncertainty propagation in Eqs. (4)–(6) in order to calculate the total uncertainties for each coordinate. This involves for example to include the uncertainty in the source position even though its position is assumed to be (0,0,0). In this study, the uncertainty propagation was performed for three real cases, corresponding to the three HPGe detector types which SALSA is specifically designed for. The distances ^{22}Na source–Ge detector (d) and Ge detector–γ camera ($d + D$) are adjusted depending on the detector size and, therefore, their uncertainties, together with the uncertainty in the estimation of the γ camera interaction point, have a different impact in the HPGe detector interaction point, the objective of SALSA.

The expected spatial resolution inside the HPGe crystal for each coordinate is summarized in Table 3. As expected, total uncertainty is largely driven by the uncertainty in the Z coordinate (X in S_2), pointing in the direction from HPGe crystal to the γ camera. Therefore, the greater the distance D with respect to d, the better the spatial resolution in the position determination in the HPGe crystal. The large detection surface in our γ camera allows us to move it away with respect to the ^{22}Na source and reduce the distance from the ^{22}Na source to the HPGe detector (d), increasing the spatial resolution of the system.

Table 3
Expected spatial resolution for points inside the HPGe crystal.

Detector	σ_{X_D} (mm)	σ_{Z_D} (mm)	σ_{Y_D} (mm)
BEGe	± 1.08	± 1.08	± 0.98
PLANAR	± 0.92	± 0.92	± 0.94
AGATA	± 2.05	± 2.05	± 1.84

8. Validation of the position determination with SALSA

A test was performed using a conventional Broad Energy HPGe detector, model BEGe 8030 by CANBERRA. A X-ray radiography was taken to this coaxial detector to measure accurately its size, this being 30-mm height and 80-mm diameter. Two scanning setups were used for this purpose: the SALSA scanning table running as explained along this paper (see Fig. 2), this setup being referred to as Imaging mode from now on, and a new setup using the elements of SALSA to calculate interactions positions applying the Compton effect, this one being referred to as Compton mode. The setup corresponding to the Compton mode is made of the ^{22}Na source described in Section 3, which is collimated with a 50 mm diameter and 50 mm height cylindrical collimator with a 1 mm diameter hole along its central axis. This collimator is positioned by means of a 0.1 mm precision XZ positioning system on the centre of the detector window. The γ camera is facing the detector on the YZ plane, as shown in Fig. 10. In both setups, the BEGe detector position is checked with a 1-mm-dot laser. Measurements were acquired in coincidence between γ camera and Ge detector in order to record those events that scatter in the Ge detector and impact afterwards in the γ camera. Together with the readout electronics associated to the γ camera and described in [17], a flash analogue-to-digital converter (FADC) with 12 bits dynamic range and 100 MS/s sampling rate, model SIS3302-ADC, by Struck was used to acquire the digitized BEGe detector pulses in both Imaging and Compton modes. In order to increase the time accuracy, a cubic spline interpolation method was applied to the recorded Ge pulse shapes [20]. FADC sample rates increased from 1 sample each 10 ns to 1 sample per 1 ns by using this mathematical model. The interpolation allows a better time resolution in the validation study presented in this work.

From all the in-coincidence events acquired in the Compton mode, only the ones scattered at 90° in the Ge crystal were selected by making an energy window in the BEGe spectrum at 255.5 keV energy deposited in a 90° scattering of 511 keV photons from ^{22}Na disintegrations. The 1274.54 keV emission from the ^{22}Na was not utilized given that there are actually more γ rays that

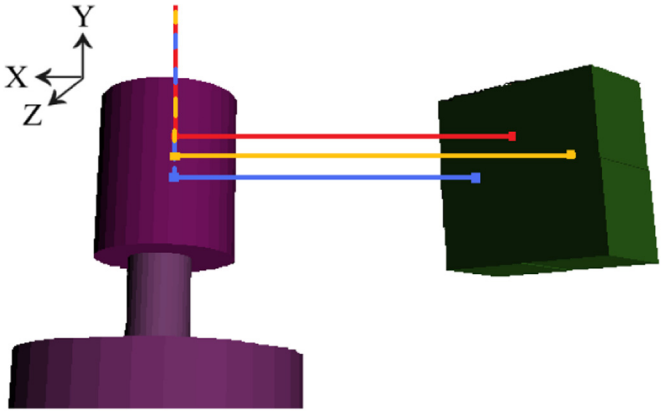

Fig. 10. Schematics for SALSA working in Compton mode. The 1-mm-diameter collimated ^{22}Na source delivers γ rays that are detected in the γ camera after a 90° Compton scattering.

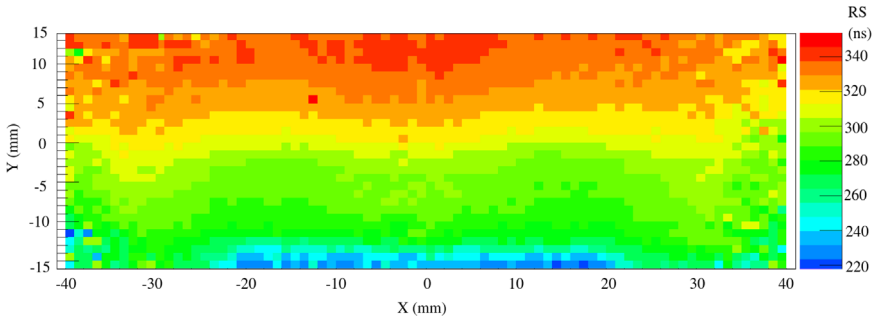

Fig. 11. Rise times (RS) of the Ge pulses on the *XY* projection of the BEGe detector when SALSA works in imaging mode. The rear contact is placed in the $X=0$ mm, $Y=-15$ mm position, while the front contact is located along the $Y=15$ mm line. (For interpretation of the references to colour in this figure caption, the reader is referred to the web version of this paper.)

manage to pass through the collimator and then going to Ge crystal and then to the γ-camera after a Compton scattering than γ rays that pass through the 1 mm collimation hole without interaction with the Pb absorber and then going to Ge crystal and then to the γ-camera after a Compton scattering. For that reason we need to quantify this ratio. With this goal, a Monte Carlo simulation was performed on the basis of the complete setup presented in Fig. 10. In the simulation all the events were tracked in order to know whether they interact with the Pb absorber, with the Ge crystal or with the LYSO crystal. For each event, every interaction position and the deposited energy were recorded. With this information, for 511 keV γ-rays, the simulation has given a result of 59% of the events passing through the collimator hole versus the 41% of the events that manage to pass through the Pb collimator, with and without interaction with the Pb. One conclusion we have got from the simulation is that from the 41% of the events that manage to pass through the Pb collimator, only the ones having a Compton scattering and depositing low energy will disturb our experimental results given that the ones depositing high energy will have bigger Compton angle and the vertical coordinate between γ-camera and Ge crystal will be incoherent. In the case of the γ-rays passing without interaction through the Pb and then having a 90° Compton scattering, the ones that will enter in our energy gate, the situation of the vertical coordinate will be incoherent as well. Therefore, we can reject these events in our analysis increasing our ratio of good events, the ones that has a 90° Compton scattering in the Ge crystal and then travel to the γ-camera, versus the ones that have the same sequence but after a Compton scattering in the Pb collimator, from 59% up to 77% for 511 keV γ rays. For this emission, the energy resolution of our BEGe detector at that energy is 0.81 keV. However, the energy window width is chosen to include events at $(90 \pm 1)^\circ$ Compton angles in order to get a balance between statistics and reliability. This interval totally comprises the BEGe energy resolution and the uncertainty in the incident photon direction, which comes from the uncertainty in the collimated emission position, the beam divergence resulting from the finite collimator dimensions and the uncertainty in the location of the centre of the detector. Thereby, the energy gate used in the Ge spectrum corresponds to $\Delta_{511} = 255.5^{+2.2}_{-2.3}$ keV. After the energy gating, data were refined by selecting those events that occurred within the condition of fold-1, i.e., that only one interaction occurred in the Ge crystal. This selection is based on the Pulse Shape Analysis (PSA) of each pulse [21].

The interaction position in the Ge crystal of a particular event was obtained in the Compton mode from the mechanical collimated position of the ^{22}Na source placed on the plane of the Ge window, which corresponds to the *X* and *Z* coordinates as shown in Fig. 10. The interaction point of the 90° scattered γ ray in the γ camera provided the *Y* coordinate. Thereby, the Compton mode enabled for determining the Ge interaction position in an alternative way to SALSA and, consequently, provided a suitable validation of the SALSA position determination. In order to proceed with this validation, a comparison between the results obtained with both setups was performed. Specifically, electrical pulses from the BEGe detector corresponding to γ rays interacting within a 2-mm-diameter and 3-cm-long cylindrical column going from the bottom to the top of the Ge crystal and centred on its main axis were taken into account in the comparison. The selection was carried out by taking the positions provided by the PSD in the imaging mode. Actually, the volume of the crystal illuminated in the Compton mode when placing the collimated ^{22}Na source on the detector window, right in the central position of the crystal, is a cone of 1 mm diameter at the top and 2.2 mm at the bottom where the thick semi-punctual crystal contact is located. But, this cone is almost totally contained within the cylinder, except in the contact zone where the recovered pulses were absent.

Rise times of the Ge pulses obtained from the scanning with SALSA in imaging mode were directly associated to positions in the γ camera. The projection of the BEGe crystal on the *XY* plane of the PSD in the S_1 scanning position is shown in Fig. 11, where rise times corresponding to each position are given by means of a colour scale. Rise time increases when moving away from the rear contact as seen in Fig. 11. Therefore, it is more influenced by the *Y* coordinate of the interaction position. The accurate positioning of the BEGe detector was also checked through Fig. 11.

Ninety four pulses of the whole set acquired with SALSA in imaging mode came from the central 2-mm-diameter column of the HPGe crystal, as given by the PSD, their corresponding interaction position coordinates being calculated with the SALSA algorithm described in Section 3. Their shapes, which were also available for the comparison together with the calculated interaction positions, are shown in Fig. 12. In total 13 pulses in turn were available from the Compton mode for the comparison as

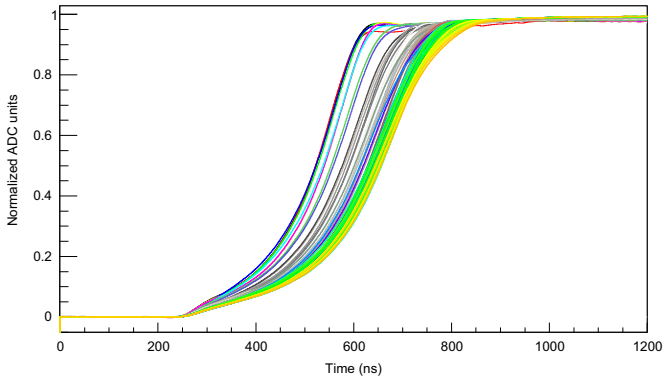

Fig. 12. Electrical pulses from the central column in the BEGe detector when SALSA works in imaging mode.

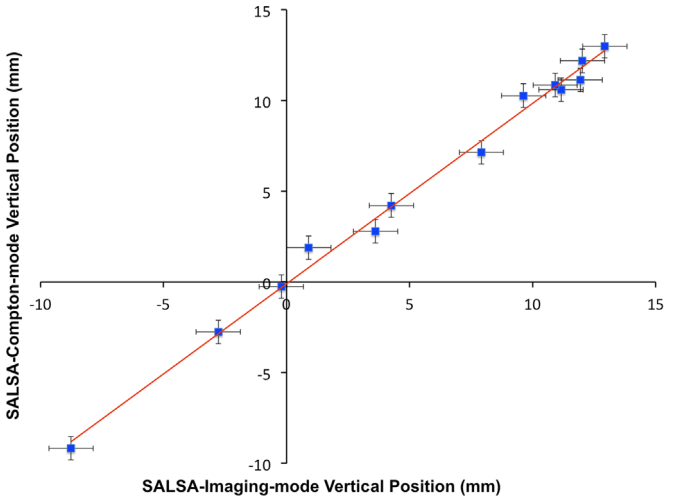

Fig. 13. Comparison between SALSA (imaging mode) and Compton-mode *Y* positions. The vertical *Y* coordinate obtained in imaging mode is represented in the *X*-axis versus the vertical *Y* coordinate in Compton mode (*Y*-axis). (For interpretation of the references to colour in this figure caption, the reader is referred to the web version of this paper.)

placed by setup construction into the 2-mm-diameter imaginary cylinder. A statistical comparison was performed between the two set of pulses. But, previously, all the pulses were aligned on an event-by-event basis at 10% of their maximum amplitude (t_{10}), as the FADC cards and the γ camera readout electronics did not have a global clock, and just the pulse data from t_{10} to t_{90} was kept. Then, each Compton pulse was compared in terms of shape with all the SALSA pulses, making a pair with the most similar one. The ROOT's Chi2Test method [22] was employed for this task. The matching of the vertical *Y* coordinates of each pair of pulses obtained from the χ^2 comparison is shown in Fig. 13, where the reconstructed *Y* coordinate from SALSA is plotted versus the corresponding one in the Compton mode. Uncertainties are also represented for each point by means of error bars, SALSA uncertainties being estimated as explained above and Compton-mode uncertainties being determined from the uncertainty in the position determination with the γ camera. A red line is drawn in Fig. 13 representing the ideal behaviour. It is worth to remark that all the uncertainties embraced the fitted line. This fact tells us the uncertainty estimation to be suitable and, therefore, the assumption to consider negligible the uncertainties introduced by the PSAC algorithm to be proper in the frame of this study. Finally, the mean deviation of the calculated positions was 0.41 mm, while the maximum one corresponds to 0.98 mm, these values being lower than the uncertainty estimated for the *Y* coordinate with SALSA, which means the *Y* coordinate calculated with the SALSA algorithm do not differ from the reference one.

9. Conclusion

The expected spatial resolution in our scanning system for different types of HPGe detectors has been studied. To accomplish this task, we took into account all the sources of uncertainty present in the determination of the interaction position of the γ ray inside the HPGe crystal. The spatial resolution was approximately 1 mm for Ge-planar and BEGe detectors and around 2 mm for AGATA detector. This improves the accuracy of the current scanning systems by a factor of 2, enhancing the scanning capabilities and allowing the relationship between the γ-ray interaction position and the electrical response in this type of detectors to be explored in detail. The position calculation performed by SALSA has been checked by using the characterization of a non-segmented HPGe crystal, for which rise time of pulses depend mainly on the *Y* coordinate. Therefore, the results reveal a proper estimation with SALSA of the *Y* positions and their uncertainties. Next studies are planned to fully characterize a segmented Ge detector.

Acknowledgement

This work has been partially supported by MICINN and Mineco through the Grants FPA2008-06419 and FPA2011-03774 and Consolider CSD2007-00042 by the Government of Spain and from Junta de Castilla y León through excellence Grant GR12.

References

[1] S. Akkoyun, et al., Nucl. Instrum. Methods A 668 (2012) 26.
[2] Official GRETA homepage ⟨http://greta.lbl.gov⟩.
[3] P. Suetens, Fundamentals of Medical Imaging, Cambridge University Press, Cambridge, 2009 (Chapter 5).
[4] F.C.L. Crespi, et al., Nucl. Instrum. Methods A 593 (2008) 440.
[5] C. Domingo-Pardo, et al., Nucl. Instrum. Methods A 643 (2011) 79.
[6] N. Goel, et al., Nucl. Instrum. Methods A 700 (2013) 10.
[7] M. Doncel, et al., J. Instrum. 10 (2015) P06010.
[8] Eckert and Ziegler Co. Sources for Medical Imaging. Available online at: ⟨http://www.ezag.de/zentralkatalog/3_sources_medical_imaging_equipment.pdf⟩.
[9] L. Pidol, et al., IEEE Trans. Nucl. Sci. NS-51 (2006) 1084.
[10] S. De Benedetti, et al., Phys. Rev. 77 (1950) 205.
[11] K.L. Erdman, Proc. Phys. Soc. A 68 (1955) 304.
[12] Available online at: ⟨http://www.hepcomotion.com/⟩.
[13] Douglas C. Montgomery, George C. Runger, Applied Statistics and Probability for Engineers, John Wiley and Sons, Inc., 2003 (Chapter 15).
[14] S. Agostinelli, et al., Nucl. Instrum. Methods A 506 (2003) 250.
[15] J. Allison, et al., IEEE Trans. Nucl. Sci. NS-53 (2006) 270.
[16] Wolfram Mathematica™ 8.
[17] A. Hernandez-Prieto, B. Quintana, IEEE Trans. Nucl. Sci. NS-60 (2013) 4719.
[18] W.L. Deemer, D.F. Votaw, Ann. Math. Stat. 26 (1955) 498.
[19] F.M. Al-Athari, J. Math. Stat. 4 (2008) 284.
[20] William H. Press, et al., Numerical Recipes: The Art of Scientific Computing, 3rd ed., Cambridge University Press, Cambridge, 2007.
[21] F.C.L. Crespi, et al., Nucl. Instrum. Methods A 570 (2007) 459.
[22] Available online at: ⟨http://root.cern.ch/root/html/TH1.htmlt⟩.